Proceedings of HT2005
2005 ASME Summer Heat Transfer Conference
San Francisco, California, USA, July 17-22, 2005

DRAFT HT2005-72643

EFFECTIVE OPTICAL PROPERTIES OF NANOPOROUS SILICON

Matt Braun and Laurent Pilon*

Department of Mechanical and Aerospace Engineering
University of California
Los Angeles, California 90025
Email: pilon@seas.ucla.edu

ABSTRACT

Nanoporous materials consist of nanosize voids embedded in a solid matrix. The pores can be closed or open and have various shapes and sizes. Their applications range from optical and optoelectronics devices to biosensors. In order to effectively utilize and characterize nanoporous media for these various applications, models that describe their effective optical properties are necessary. Numerous effective medium models have been proposed. However, validations of these models against experimental data are often contradictory and inconclusive. This issue was numerically investigated by solving the two-dimensional Maxwell's equations in absorbing nanoporous silicon thin-films. All interfaces are assumed to be optically smooth and characteristic pore size is much smaller than the wavelength of incident radiation so electromagnetic wave scattering by pores can be safely neglected. The envelope method was then used to retrieve the effective index of refraction and absorption index from the computed transmittance. The numerical results agree very well for both the index of refraction and the absorption index with a recent model obtained by applying the Volume Averaging Theory (VAT) to the Maxwell's equations. However, commonly used models such as the Maxwell-Garnett, Bruggeman, parallel, and series models systematically and sometimes significantly underpredict the numerical results.

NOMENCLATURE

A, B variables in Equations (9) and (10).
c speed of light.
$\vec{E}$ electric field vector.
$\vec{H}$ magnetic field vector.
k absorption index.
L thickness of a thin-film.
m complex index of refraction, $m = n - ik$.
n real part of the complex index of refraction.
$\vec{n}$ normal vector.
t time.
T transmittance.
N variable in Equation (28).
x x-direction.
y y-direction.
z z-direction.
ε electric permitivity.
ϕ porosity.
λ wavelength of the electromagnetic wave.
μ magnetic permeability.
$\vec{\pi}$ Poynting vector.
σ electrical conductivity.
ω angular frequency of electromagnetic wave (rad/s).

Subscript

0 refers to vacuum, or an incident property.
1 refers to surroundings in thin-film system.
2 refers to thin-film in thin-film system.
3 refers to substrate in thin-film system.
avg refers to time-averaged value.
c refers to continuous phase.
d refers to dispersed phase (nanopores).

*Address all correspondence to this author.

Copyright © 2005 by ASME

eff refers to effective properties.
max refers to envelope of maximum transmittance.
min refers to envelope of minimum transmittance.
x refers to x-direction.
y refers to y-direction.
z refers to z-direction.
c continuous phase.
d dispersed phase.
λ wavelength.

INTRODUCTION

In recent years, porous silicon made by electrochemical etching of doped single crystal silicon has been the subject of intense study. Potential applications include biosensors [1–3] and optical devices including waveguides [4–6], Bragg reflectors [7–13], and Fabry-Perot filters [7, 9, 11, 12, 14]. These optical devices take advantage of interferences and total reflection caused by differences in optical properties between adjacent media. For example, in order to confine and propagate electromagnetic radiation within a waveguide, the guide region itself must have a higher index of refraction than the surrounding cladding [15]. Bragg reflectors and Fabry-Perot filters are built by generating alternating layers with prescribed thickness and index of refraction. This geometry uses constructive and destructive interferences to selectively reflect or transmit at desired wavelengths. In each of these optical applications, the index of refraction is tuned by controlling the morphology and porosity of the nanosize voids. Optimizing the performance of a given component requires accurate knowledge of the effect of porosity and of each phase on the overall optical properties of the nanoporous medium. Numerous effective medium models treating heterogeneous media as homogeneous media with some effective properties have been suggested. However, validation of the various models against experimental data often yields contradictory results [16].

The present study aims at numerically simulating electromagnetic wave transport in nanoporous silicon. In particular, spectral transmittance and reflectance are computed and used to retrieve the effective index of refraction and absorption index. The numerical results are then compared with the effective medium models.

CURRENT STATE OF KNOWLEDGE

Numerous effective media models have been suggested including (1) the Maxwell-Garnett Theory [17], (2) the Bruggeman effective medium approximation [18], (3) the parallel and (4) series models, and (5) those recently derived from the volume averaging method [19, 21].

The Maxwell-Garnett Theory (MGT) [17] was first developed to model the effective electric permittivity of heterogeneous media consisting of *monodispersed* spheres arranged in a cubic lattice structure within a continuous matrix and of diameter much smaller than the wavelength of the incident EM wave. Then, the effective dielectric constant $\varepsilon_{r,eff}$ is expressed as,

$$\varepsilon_{r,eff} = \varepsilon_{r,c}\left[1 - \frac{3\phi(\varepsilon_{r,c} - \varepsilon_{r,d})}{2\varepsilon_{r,c} + \varepsilon_{r,d} + \phi(\varepsilon_{r,c} - \varepsilon_{r,d})}\right] \tag{1}$$

where $\varepsilon_{r,c}$ and $\varepsilon_{r,d}$ are the dielectric constants of the continuous and dispersed phases, respectively, while ϕ is the porosity. Moreover, the MGT model is not valid over the entire range of porosities since the spheres start overlapping for porosity values of $\pi/6 \simeq 52\%$ for 3D cubic lattice arrangement.

To address this issue, Bruggeman [18] considered a similar situation of *polydispersed* spheres distributed in a continuous medium. The effective property $\varepsilon_{r,eff}$ is obtained by solving the following implicit equation,

$$1 - \phi = \frac{(\varepsilon_{r,eff}/\varepsilon_{r,c} - \varepsilon_{r,d}/\varepsilon_{r,c})}{\left[\left(\frac{\varepsilon_{r,eff}}{\varepsilon_{r,c}}\right)^{1/3}(1 - \varepsilon_{r,d}/\varepsilon_{r,c})\right]} \tag{2}$$

Despite applicability to the full range of porosity ($0 \leq \phi \leq 1$) [20], Bruggeman's model is not used as often as MGT in the literature.

Other commonly encountered models are the parallel and series models. The parallel model gives the effective property ψ_{eff} as a linear function of the properties of the continuous and dispersed phases, i.e.,

$$\psi_{eff} = (1 - \phi)\psi_c + \phi\psi_d \tag{3}$$

The series model on the other hand, gives

$$\frac{1}{\psi_{eff}} = \frac{1 - \phi}{\psi_c} + \frac{\phi}{\psi_d} \tag{4}$$

A more rigorous approach, albeit more mathematically involved, was recently derived [19, 21] by applying the volume averaging theory (VAT) to the Maxwell's equations. The authors predicted the effective dielectric constant $\varepsilon_{r,eff}$, relative permeability $\mu_{r,eff}$, and electrical conductivity σ_{eff} of a two-phase mixture of arbitrary morphology as [19],

$$\varepsilon_{r,eff} = (1 - \phi)\varepsilon_{r,c} + \phi\varepsilon_{r,d} \tag{5}$$

$$\sigma_{eff} = (1 - \phi)\sigma_c + \phi\sigma_d \tag{6}$$

The range of validity of these expressions, and a set of inequalities to be satisfied was developed [19, 21]. The authors conclude

Copyright © 2005 by ASME

that "the constraints [posed by these inequalities] are very severe and are not satisfied for many processes."

Moreover, all the above models disregard the shape, the size distribution, and/or the spatial distribution of the pores. However, these characteristics were stated to affect the effective properties of the heterogeneous medium [22, 23]. Attempts have been made to account for non-spherical cell geometry by modifying the Maxwell-Garnett [24] and the Bruggeman [25, 26] models. For example, Schultz [26] generalized the Bruggeman model for dispersions of randomly oriented spheroids. This model also accounts for the orientation of the cells by incorporating the angle between the revolution axis of the spheroid and the incident energy direction. Models such as these are difficult to use in practice because they require specific knowledge of the shape and orientation of the cells.

Finally, note that the above models have been used to predict properties for which they were not necessarily derived. For example, the MGT model developed for the electric permittivity ε has been used for the index of refraction [27, 28] and for the thermal conductivity (see Ref.[[20]] and references therein). Overall, it is not always clear to the user which model is the most appropriate for any particular situation and property. Experimental data could be used to evaluate the various models, however, the conclusions drawn can be contradictory [16]. For example, Si *et al*. [29] concluded that the series model best describes the dielectric constant of nanoporous silica thin-films with uniformly distributed closed voids. Krause *et al*. [22], on the other hand, concluded that the Maxwell-Garnett model is more appropriate for polymeric closed-cell nanofoam. This apparent contradiction may be attributed to the difficulties and uncertainties in measuring the film porosity, the pore size and shape, and also the optical properties of a nanoporous thin-film. To address this issue, the present study aims at numerically simulating EM wave transport in non-absorbing nanoporous media in order to determine: (1) the range of validity of the effective medium approach and (2) the most appropriate effective property model for the dielectric constant and for the index of refraction of non-absorbing nanoporous media.

ANALYSIS

Optical Properties from Volume Averaging Theory

For a homogeneous material the index of refraction n and the absorption index k can be written in terms of the real part of the dielectric constant ε_r and of the electrical conductivity σ as [15],

$$n^2 = \frac{1}{2}\left[\varepsilon_r + \sqrt{\varepsilon_r^2 + \left(\frac{\lambda\sigma}{2\pi c_0 \varepsilon_0}\right)^2}\right] \tag{7}$$

$$k^2 = \frac{1}{2}\left[-\varepsilon_r + \sqrt{\varepsilon_r^2 + \left(\frac{\lambda\sigma}{2\pi c_0 \varepsilon_0}\right)^2}\right] \tag{8}$$

where λ is the wavelength of the incident radiation, c_0 is the speed of light in vacuum, and ε_0 is the permittivity of free space. The expression derived by Del Rio and Whitaker [19] for the effective dielectric constant $\varepsilon_{r,eff}$ and electrical conductivity σ_{eff} of a two-phase nanoporous medium [Equations (5) and (6)] can be used to express the effective optical properties of a two-phase nanocomposite material as,

$$n_{eff}^2 = \frac{1}{2}\left[A + \sqrt{A^2 + B^2}\right] \tag{9}$$

$$k_{eff}^2 = \frac{1}{2}\left[-A + \sqrt{A^2 + B^2}\right] \tag{10}$$

where

$$A = \varepsilon_{r,eff} = \phi(n_d^2 - k_d^2) + (1-\phi)(n_c^2 - k_c^2) \tag{11}$$

and

$$B = \frac{\lambda\sigma_{eff}}{2\pi c_0 \varepsilon_0} = 2n_d k_d \phi + 2n_c k_c (1-\phi) \tag{12}$$

Governing Equations and Numerical Implementation

In order to develop the numerical model let us first consider a surrounding environment (medium 1, n_1, $k_1 = 0$) from which the incident electromagnetic wave is incident on an absorbing thin-film (medium 2, n_2, k_2) deposited onto an absorbing dense substrate (medium 3, n_3, k_3). A linearly polarized plane wave in transverse electric (TE) mode is incident normal to the film top surface and propagates through the two-dimensional thin-film along the x-direction (see Figure 1). As the wave propagates in the x-y plane, it has only one electric field component in the z-direction, while the magnetic field has two components in the x-y plane (i.e. perpendicularly polarized), such that in a general time-harmonic form,

$$\vec{E}(x,y,t) = E_z(x,y)e^{i\omega t}\vec{e}_z \tag{13}$$

and

$$\vec{H}(x,y,t) = [H_x(x,y)\vec{e}_x + H_y(x,y)\vec{e}_y]e^{i\omega t} \tag{14}$$

Here, $\vec{E}$ is the electric field vector, $\vec{H}$ is the magnetic field vector, and $\omega = 2\pi c_0/\lambda$ is the angular frequency of the wave. For general time-varying fields in a conducting medium, the Maxwell's

Copyright © 2005 by ASME

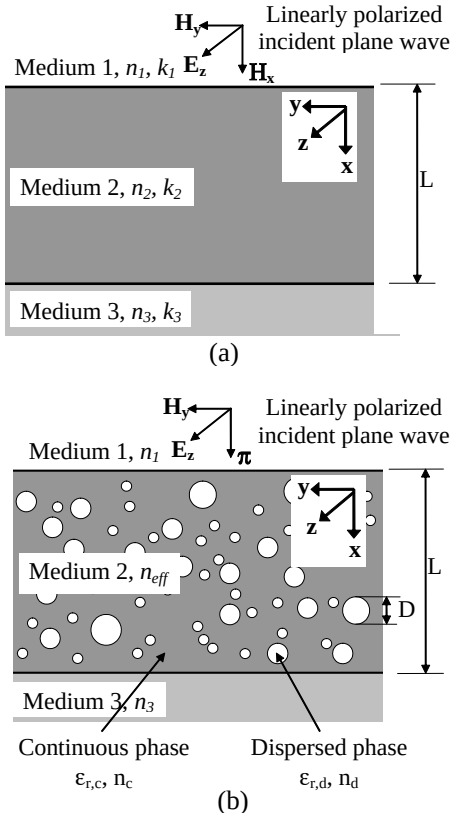

Figure 1. SCHEMATIC OF TWO-DIMENSIONAL (a) DENSE AND (b) POROUS SILICON THIN-FILM EXPOSED TO A LINEARLY POLARIZED PLANE WAVE.

Equations can be written as,

$$\frac{1}{\mu_r\mu_0}\nabla\times[\nabla\times\vec{E}(x,y,t)]-\omega^2\varepsilon_r^*\varepsilon_0\vec{E}(x,y,t)=0 \qquad (15)$$

$$\frac{1}{\varepsilon_r^*\varepsilon_0}\nabla\times[\nabla\times\vec{H}(x,y,t)]-\omega^2\mu_r\mu_0\vec{H}(x,y,t)=0 \qquad (16)$$

where μ_0 and μ_r are the magnetic permeability of vacuum and the magnetic relative permeability, respectively, while ε_r^* ($= n^2-k^2-i2nk$) is the complex dielectric constant. The associated boundary conditions are,

$$\vec{n}\times(\vec{H}_1-\vec{H}_2)=0 \quad \text{at the surroundings-film interface} \qquad (17)$$

$$\vec{n}\times\vec{H}=0 \quad \text{at symmetry boundaries} \qquad (18)$$

$$\frac{\mu_0^{1/2}}{\varepsilon_0^{1/2}}(\vec{n}\times\vec{H})+(\varepsilon_r^*)^{1/2}\vec{E}=0 \text{ at the film-substrate interface} \qquad (19)$$

$$\frac{\mu_0^{1/2}}{\varepsilon_0^{1/2}}(\vec{n}\times\vec{H})+\varepsilon_r^{*1/2}\vec{E}=2\varepsilon_r^{*1/2}\vec{E}_0 \quad \text{at the source surface} \qquad (20)$$

where $\vec{n}$ is the normal vector to the appropriate interface. Equation (19) corresponds to a semi-infinite substrate while Equation (20) models the source surface where the incident electromagnetic wave $\vec{E}_0$ is emitted and that is transparent to the reflected waves.

Moreover, the Poynting vector $\vec{\pi}$ is defined as the cross product of the electric and magnetic vectors, $\vec{\pi}=\vec{E}\times\vec{H}$. Its magnitude corresponds to the energy flux carried by the propagating electromagnetic wave. Solving Maxwell's equations for the nonzero component of the electric field vector E_z, and relating it to the magnetic field yields,

$$H_y=\frac{n}{\mu_r\mu_0 c_0}E_z \qquad (21)$$

Averaging the Poynting vector over an appropriate time interval yields [15],

$$|\pi|_{avg}=\frac{n}{2\mu_r\mu_0 c_0}|E_z|^2_{avg} \qquad (22)$$

The incident electric field E_{0z} and therefore the incident time-averaged Poynting vector $|\pi_0|_{avg}$ are imposed at all locations along the source surface. The values of the Poynting vector along the film-substrate interface are then calculated numerically and averaged along the boundary to yield $|\pi_t|_{avg}$. The transmittance of the thin-film is then recovered by taking the ratio of the transmitted to the incident average Poynting vectors, i.e, $T_{film}=|\pi_t|_{avg}/|\pi_0|_{avg}$. Similarly, the magnitude of the reflected time-averaged Poynting vector $|\pi_r|_{avg}$ is computed numerically, and the reflectance of the film is computed according to $R_{film}=|\pi_r|_{avg}/|\pi_0|_{avg}$.

Finally, the above equations were solved numerically using a commercially available finite element solver (FEMLAB 3.0) applying the Galerkin finite element method on unstructured meshes. The two-dimensional Maxwell's equations are solved in the frequency domain using a 2D transverse electric (TE) wave formulation as described by Equation (13). In particular, the discretization uses second order elements to solve for the electric field.

In order to validate the numerical implementation of this system of equations, a system composed of a dense absorbing film ($n_2=1.7$, k_2) of thickness L deposited on a perfectly reflective substrate ($n_3=k_3\to\infty$) in air ($n_1=1$, $k_1=0$) was simulated. The value of k_2 was varied over 3 orders of magnitude from 0.001 to 1, and the infinitely large optical constants of the substrate were approximated as $n_3=k_3=10^6$. Normal reflectivity of the system was computed and plotted as a function of $\pi L/\lambda$ [16]. The numerical solutions match the analytical solutions found in Ref. [15].

Copyright © 2005 by ASME

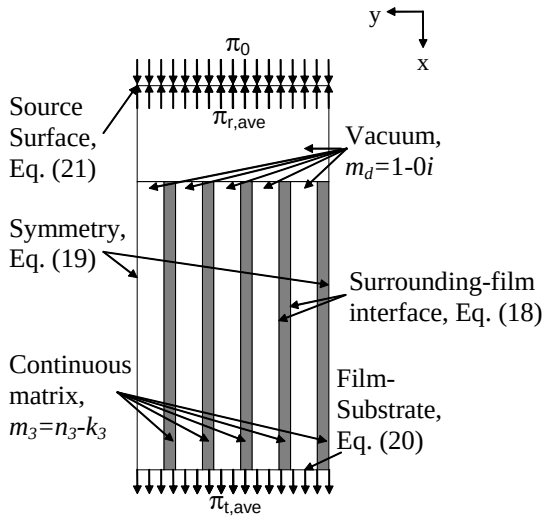

Figure 2. SCHEMATIC OF MODEL COMPOSED OF TEN ALTERNATING COLUMNS OF VACUUM AND SILICON ALONG WITH BOUNDARY CONDITIONS AND PROPERTIES.

Simulations of Porous Silicon Thin-Films

Figure 1b schematically shows the geometry of the PS thin-film on a semi-infinite silicon substrate. Polarization effects are disregarded since (1) the incident EM wave is normal to the surface, i.e., the plane of incidence is not defined and the components of the polarization cannot be distinguished [15], and (2) we assume the medium to be axisymetric so that it can be modelled as a two-dimensional structure as shown in Figure 1b. Nonlinear optical effects are neglected. We also assume that all interfaces (in the pores and at the PS surfaces) are optically smooth, i.e., surface roughness is much smaller than the incident wavelength. This may not be satisfied in practice due to the synthesis process [30–32]. Moreover, characteristic pore size is much smaller than the wavelength of incident radiation so electromagnetic wave scattering (i.e., diffraction, reflection, and refraction) by pores can be safely neglected. In addition, non-linear optical effects are neglected. Finally, surface phonon and plasmon polaritons are not observed in the current situation as resonance modes were not excited for the materials and wavelengths considered.

The Maxwell's equations are solved in both phases separately as previously described. Equation (17) is used as the boundary condition not only at the incident vacuum-film interface but also at all silicon-pore interfaces. Figure 2 is a schematic representation of an actual model consisting of 10 columnar pores alternating between silicon and vacuum corresponding to a porosity ϕ=0.70. In this specific geometric configuration, the authors showed that the effective properties can be defined for any film thickness [33]. Here, the nanoporous thin-film thickness was arbitrarily chosen to be 1 μm and the width of the silicon and vacuum columns were varied depending on the porosity. The figure also indicates material properties of the various domains and the locations at which each of the boundary conditions are applied.

It is important to note that Maxwell's equations are generally applied to macroscopic averages of the fields which can vary widely in the vicinity of individual atoms where they undergo quantum mechanical effects. These effects are neglected in the present study and all phases are treated as homogeneous and isotropic media for which index of refraction n and absorption index k are defined. This is a reasonable assumption for length scales on the order of ten lattice constants or about 5 nm (see Ref. [34] p. 387).

Index of Refraction of Silicon

Simulations were conducted for porous silicon composed of alternating parallel columns of silicon ($m_c = n_c - ik_c$) and vacuum ($m_d = 1$). The surrounding medium was also vacuum, and the substrate was bulk silicon with $m_3 = m_c = n_c - ik_c$. The optical properties of lightly doped (doping concentration $\leq 10^{15} cm^{-3}$) single crystal silicon used in the simulations were expressed as functions of wavelength λ and temperature T [35],

$$n_c(\lambda, T) = n_0(\lambda) + \gamma(\lambda) T \tag{23}$$

$$\text{where} \quad n_0(\lambda) = \sqrt{4.565 + \frac{97.3}{3.648^2 - (1.24/\lambda)^2}} \tag{24}$$

$$\text{and} \quad \gamma(\lambda) = -1.864 \times 10^{-4} + \frac{5.394 \times 10^{-3}}{3.648^2 - (1.24/\lambda)^2} \tag{25}$$

On the other hand, the expression for the absorption index is given by [35],

$$k_c(\lambda, T) = k_{0,\lambda} \exp\left[\frac{T}{369.9 - \exp(-12.92 + 6.831/\lambda)}\right] \tag{26}$$

where

$$k_{0,\lambda} = -0.0805 + \exp\left[-3.189 + \frac{7.946}{3.648^2 - (1.24/\lambda)^2}\right] \tag{27}$$

In both cases, λ is expressed in microns and T in ^{o}C. The temperature T is set to 20^{o}C. These models have been shown to provide good accuracy in the spectral interval from 400 to 840 nm and temperatures between 20 and 490^{o}C [35].

Retrieval of Effective Complex Index of Refraction

The envelop method is a straightforward and accurate method to retrieve the optical properties for weakly absorbing

Copyright © 2005 by ASME

films [36]. It takes advantage of the interference pattern displayed in the transmission spectrum of an absorbing thin-film. Two continuous functions can be deduced from the transmission spectrum: (1) $T_{min}(\lambda)$ is the envelope function of the local minima, and (2) $T_{max}(\lambda)$ is that of the local maxima. The index of refraction n_{eff} and absorption index k_{eff} of the film can then be calculated from,

$$n_{eff} = [N + (N^2 - n_1^2 n_3^2)^{1/2}]^{1/2} \tag{28}$$

$$\text{where} \quad N = \frac{n_1^2 + n_3^2}{2} + \frac{2n_1 n_3 (T_{max} - T_{min})}{T_{max} T_{min}} \tag{29}$$

and

$$k_{eff} = \frac{-\lambda}{4\pi L} \ln \frac{(n_{eff} + n_1)(n_3 + n_{eff})[1 - (T_{max}/T_{min})^{1/2}]}{(n_{eff} - n_1)(n_3 - n_{eff})[1 + (T_{max}/T_{min})^{1/2}]} \tag{30}$$

Here the subscripts 1 and 3 refer to the the media above and below the nanoporous thin-film, respectively. Validation of the envelope method combined with the simulated transmittance and reflectance was performed by retrieving the spectral complex index of refraction of a known thin-film.

The retrieved values for n_2 and k_2 fall within 0.2% and 2.5% of the input values, respectively [16]. Finally, it should be noted that if the optical constants of the thin film vary as a function of λ, the envelope method allows for the direct and accurate determination of both the effective spectral index of refraction $n_{eff}(\lambda)$ and the absorption index $k_{eff}(\lambda)$ of nanocomposite media.

RESULTS AND DISCUSSION

Effect of Porosity on the Index of Refraction

To assess the validity of the commonly used models, simulations were performed for porous silicon with various porosity and with open and closed pores of various shape, size, and spatial distribution [16, 33]. The conclusions drawn can be listed as follows:

1. There exists a critical film thickness L_{cr} below which the effective index of refraction is a function of (i) the film thickness, (ii) the pore shape, (iii) their size, (iv) their spatial distribution, and (v) the wavelength considered. For film thicknesses less than L_{cr}, the effective medium approach is not applicable and the heterogeneous nature of the medium should be taken into account.
2. For films thicker than the critical thickness L_{cr}, the effective medium approach is valid and an effective index of refraction can be defined only as a function of porosity ϕ and of the indices of refraction of the constituent phases. In other words, *the pore shape, size, and spatial distribution have no effect on the effective index of refraction of the nanoporous medium*.
3. For porous silicon with columnar pores, the retrieved index of refraction is independent of the film thickness and pore size and the effective medium approximation is always valid.

For silicon, the incident wavelength was chosen to be λ = 2.71 μm at which the complex index of refraction is $m_{Si} = 3.44 - i2.5 \times 10^{-9}$ [15]. Thus, the absorption coefficient can also safely be neglected. Figure 3 shows the converged values of the effective index of refraction plotted versus porosity along with predictions of the above discussed models. The predictions from Bruggeman model differed from the MGT model by a maximum of only 2.3%. Thus, the Bruggeman model will not be discussed further.

The numerical values retrieved for n_{eff} match those predicted by the volume averaging technique [Equation (7)] within rounding error. The relative difference between the parallel, Maxwell-Garnett, and series models and the numerical results for porous silicon was up to 16.4%, 22.4%, and 39.5%, respectively. Thus, the common models described by Equations (1) to (4) should not be used for predicting the effective index of refraction of nanoporous silicon regardless of the pore geometry.

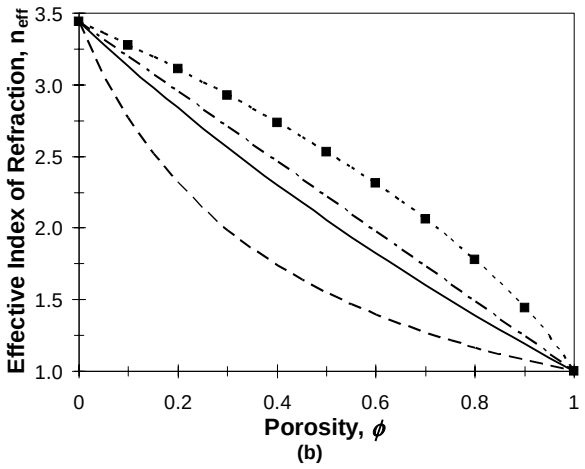

Figure 3. NUMERICAL RESULTS FOR THE EFFECTIVE INDEX OF REFRACTION OF POROUS SILICON AT λ = 2.71 μm AS A FUNCTION OF POROSITY.

Numerical Validation of the VAT Model

Using the above procedure, simulations of electromagnetic wave transport in porous silicon (PS) were conducted for various porosities. For the sake of simplicity, porous silicon with colum-

Copyright © 2005 by ASME

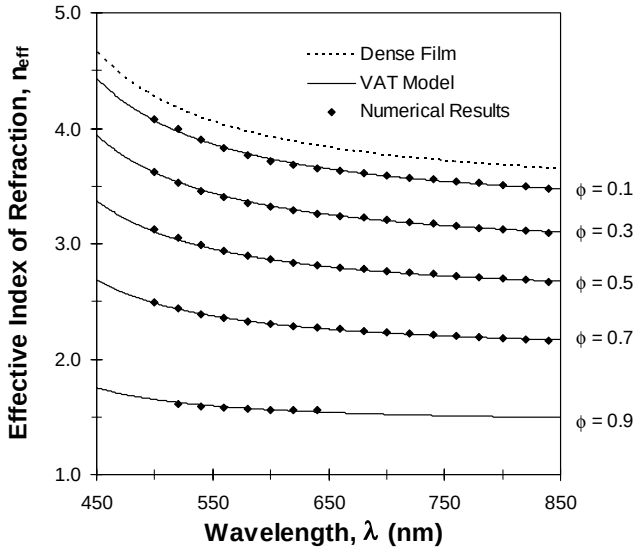

Figure 4. EFFECTIVE INDEX OF REFRACTION OF POROUS SILICON WITH VARIOUS POROSITIES AS A FUNCTION OF WAVELENGTH.

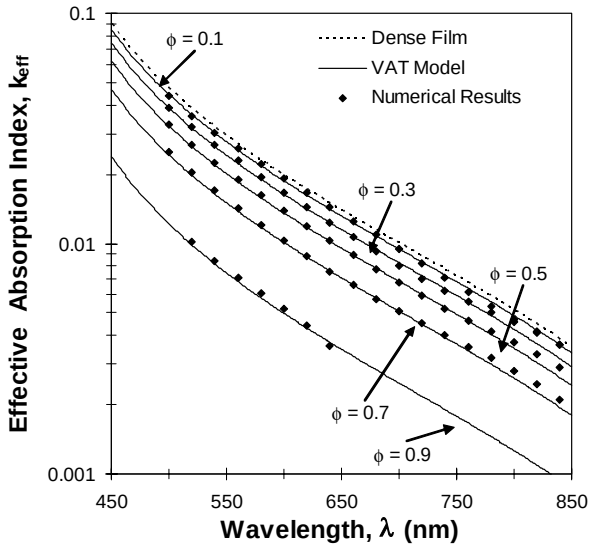

Figure 5. EFFECTIVE ABSORPTION INDEX OF POROUS SILICON WITH VARIOUS POROSITIES AS A FUNCTION OF WAVELENGTH.

nar pores was simulated as the simulations converge faster than for other pore morphology.

Optical properties of dense silicon reported by Jellison and Modine over the spectral region from 240 nm to 840 nm [35] were used. The envelope method was used to retrieve the effective index of refraction n_{eff} and absorption index k_{eff}. Figures 4 and 5 show the evolution of the effective index of refraction $n_{eff}(\lambda)$ and absorption index $k_{eff}(\lambda)$ as functions of wavelength λ for several values of porosity ϕ. The solid curves correspond to the VAT models given by Equations (9) and (10). The data points represent the values retrieved from the numerically computed transmittance using the envelope method. It is clear that the VAT model provides an accurate prediction of the effective optical properties of porous silicon. The slight deviation between numerical results and the VAT predictions for $k_{eff}(\lambda)$ at larger wavelengths can be attributed to the error associated with the envelope method and more specifically to the accuracy of the $T_{min}(\lambda)$ and $T_{max}(\lambda)$ fits. Indeed, for larger wavelengths the fringe spacing increases, and therefore the accuracy of the $T_{min}(\lambda)$ and $T_{max}(\lambda)$ fits is reduced. This can be observed for $\phi = 0.1$ where accurate $T_{min}(\lambda)$ and $T_{max}(\lambda)$ functions are obtained for wavelength less than 640 nm. In addition, at smaller wavelengths ($\lambda < 500$ nm) the magnitude of the fringes decreases to zero making inaccurate the retrieval of the optical properties. This can be attributed to the fact that the absorption index of silicon k_c increases to values on the order of 0.01, and the wavelength decreases significantly relative to the film thickness.

Figures 6 and 7 are drawn from the same data as Figures 4 and 5, but instead shows the changes in optical properties as a function of porosity at three arbitrarily chosen wavelengths namely λ = 520, 700, and 840 nm. The solid curves correspond to the VAT models, and the points to numerical results. Overall, the VAT models provide accurate predictions of the numerically retrieved effective optical properties of porous silicon.

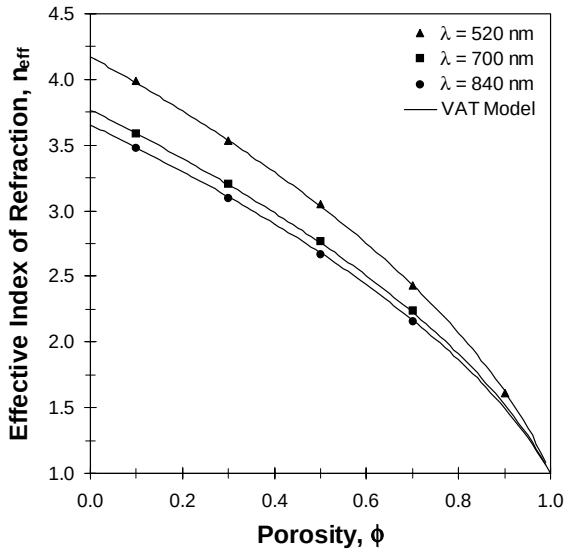

Figure 6. EFFECTIVE INDEX OF REFRACTION OF POROUS SILICON AS A FUNCTION OF POROSITY FOR DIFFERENT WAVELENGTHS EQ. (9)].

Copyright © 2005 by ASME

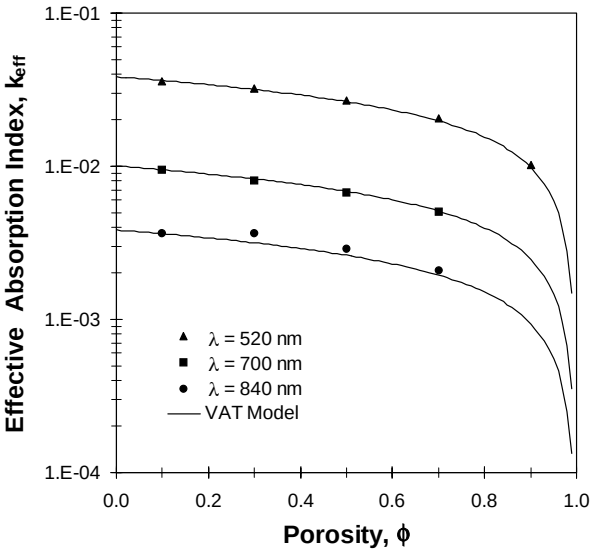

Figure 7. EFFECTIVE ABSORPTION INDEX OF POROUS SILICON AS A FUNCTION OF POROSITY FOR DIFFERENT WAVELENGTHS EQ. (10)].

CONCLUDING REMARKS

The VAT model for the effective dielectric and electrical properties of two-phase media [19] has been used to derive the effective index of refraction n_{eff} and absorption index k_{eff} of nanoporous silicon. Moreover, a numerical scheme has been developed and implemented to solve the Maxwell's equations for TE electromagnetic wave transport through porous silicon. The envelope method was then used to retrieve the effective optical properties for the simulated porous silicon. The results are in excellent agreement with the predictions made from the VAT model for the complex index of refraction. It also indirectly validate the expression for the effective dielectric constant and electric conductivity given by Equation (5) and (6), respectively. Note that this is well known for the columnar pores. However, the VAT model has been proven valid for much more complex pore geometries including spheres, ellipsoids, connected spherical pores [16, 33]. Therefore, the above results are anticipated to be valid for any pore geometries provided that the effective medium approximation is valid. Finally, the results can be extended to normally incident transverse magnetic (TM) waves as polarization effect were not considered.

REFERENCES

[1] Martin-Palma, R., Torres-Costa, V., Arroyo-Hernandez, M., Manso, M., Perez-Rigueiro, J., and Martinez-Duart, J., 2004. "Porous silicon multilayer stacks for optical biosensing applications". *Microelectronics Journal,* **35** , pp. 45–48.

[2] Arroyo-Hernandez, M., Martin-Palma, R., Perez-Rigueiro, J., Garcia-Ruiz, J., Garcia-Fierro, J., and Martinez-Duart, J., 2003. "Biofunctionalization of surfaces of nanostructured porous silicon". *Materials Science and Engineering,* **23** , pp. 697–701.

[3] Chan, S., Li, Y., Rothberg, L., Miller, B., and Fauchet, P., 2001. "Nanoscale silicon microcavities for biosensing". *Materials Science and Engineering,* **15** , pp. 277–282.

[4] Loni, A., Canham, L., Berger, M., Arens-Fischer, R., Munder, H., Luth, H., Arrand, H., and Benson, T., 1996. "Porous silicon multilayer optical waveguides". *Thin Solid Films,* **276** , pp. 143–146.

[5] Arrand, H., Benson, T., Loni, A., Krueger, M., Thoenissen, M., and Lueth, H., 1997. "Self-aligned porous silicon optical waveguides". Electronics Letters, **33** (20) , pp. 1724–1725.

[6] Jain, A., Rogojevic, S., Ponoth, S., Matthew, I., Gill, W., Persans, P., Tomozawa, M., Plawsky, J., and Simonyi, E., 2001. "Porous silica materials as low-*k* dielectrics for electronic and optical interconnects". *Thin Solid Films,* **398** , pp. 513–522.

[7] Berger, M., Thonissen, M., Arens-Fischer, R., Munder, H., Luth, H., Arntzen, M., and Thei, W., 1995. "Investigation and design of optical properties of porosity superlattices". *Thin Solid Films,* **255** , pp. 313–316.

[8] Diener, J., Künzner, N., Kovalev, D., Gross, E., Timoshenko, V., Polisski, G., and Koch, F., 2001. "Dichroic Bragg reflectors based on birefringent porous silicon". Applied Physics Letters, **78** (24) , pp. 3887–8889.

[9] Krüger, M., Marso, M., Berger, M., Thönissen, M., Billat, S., Loo, R., Reetz, W., Lüth, H., Hilbrich, S., Arens-Fischer, R., and Grosse, P., 1997. "Color-sensitive photodetector based on porous silicon superlattices". *Thin Solid Films,* **297** , pp. 241–244.

[10] Zangooie, S., Schubert, M., Trimble, C., Thompson, D., and Woollam, J., 2001. "Infrared ellipsometry characterization of porous silicon Bragg reflectors". Applied Optics, **40** (6) , pp. 906–912.

[11] Zangooie, S., Jansson, R., and Arwin, H., 1999. "Ellipsometric characterization of anisotropic porous silicon Fabry-Perot filters and investigation of temperature effects on capillary condensation efficiency". Journal of Applied Physics, **86** (2) , pp. 850–858.

[12] Mazzoleni, C., and Pavesi, L., 1995. "Application to optical components of dielectric porous silicon multilayers". Applied Physics Letters, **67** (20) , pp. 2983–2985.

[13] Kordás, K., Beke, S., Pap, A., Uusimäki, A., and Leppävuori, S., 2004. "Optical properties of porous silicon. Part II: Fabrication and investigation of multilayer structures". *Optical Materials,* **25** , pp. 257–260.

[14] Janshoff, A., Dancil, K., Steinem, C., Greiner, E., Lin, V., Gurtner, C., Motesharei, K., Sailor, M., and Ghadiri,

Copyright © 2005 by ASME

M., 1998. “Macroporous p-type silicon Fabry-Perot layers. fabrication, characterization, and applications in biosensing”. *Journal of the American Chemical Society*, **120** , pp. 12108–12116.

[15] Brewster, M., 1992. *Thermal Radiative Transfer and Properties*. John Wiley and Sons, Inc.

[16] Braun, M., 2004. Effective optical properties of nanoporous thin-films. Master’s thesis, Mechanical and Aerospace Engineering Department, University of California, Los Angeles, CA.

[17] Garnett, J. M., 1904. “Colours in metal glasses and in metallic films”. *Philosophical Transactions of the Royal Society of London, Series A*, **203** , pp. 385–420.

[18] Bruggeman, D., 1935. “Berechnung verschiedener physikalischer konstan ten von heterogenen substanzen”. *Annals of Physics (Leipzig)*, **24** , p. 636.

[19] del Rio, J. A., and Whitaker, S., 2000. “Maxwell’s equations in two-phase systems I: Local electrodynamic equilibrium”. *Transport in Porous Media*, **39** , pp. 159–186.

[20] Cernuschi, F., Ahmaniemi, S., Vuoristo, P., and Mantyla, T., 2004. “Modelling of thermal conductivity of porous materials: application to thick thermal barrier coatings”. *Journal of the European Ceramic Society*, **24** , pp. 2657–2667.

[21] del Rio, J. A., and Whitaker, S., 2000. “Maxwell’s equations in two-phase systems II: Two-equation model”. *Transport in Porous Media*, **39** , pp. 259–287.

[22] Krause, B., Koops, G., van der Vegt, N., Wessling, M., Wubbenhorst, M., and van Turnhout, J., 2002. “Ultralow-k dielectrics made by supercritical foaming of thin polymer films”. Advanced Materials, **14** (15) , pp. 1041–1046.

[23] Cha, H., Hedrick, J., DiPietro, R., Blume, T., Beyers, R., and Yoon, D., 1996. “Structures and dielectric properties of thin polyimide films with nanofoam morphology”. Applied Physics Letters, **68** (14) , pp. 1930–1932.

[24] Grimvall, G., 1986. *Thermophysical Preperties of Materials. Selected Topics in Solid State Physics, Vol. XVIII*. North-Holland Physics Publishing.

[25] Meredith, R., 1959. *Studies in the conductivites of dispersions*. Lawrence Radiation Laboratory Report, UCRL-8667.

[26] Schulz, B., 1981. “Thermal conductivity of porous and highly porous materials”. *High Temperatures - High Pressures*, **13** , p. 649.

[27] Labbe-Lavigne, S., Barret, S., Garet, F., Duvillaret, L., and Coutaz, J., 1998. “Far-infrared dielectric constant of porous silicon layers measured by terahertz time-domain spectroscopy”. *Journal of Applied Physics*, **83** , pp. 6007–6010.

[28] Himcinschi, C., Friedrich, M., Murray, C., Streiter, I., Schulz, S., Gessner, T., and Zahn, D., 2001. “Characterization of silica xerogel films by variable-angle spectroscopic ellipsometry and infrared spectroscopy”. Semiconductor Science & Technology, **16** (11) , pp. 806–811.

[29] Si, J., Ono, H., Uchida, K., Nozaki, S., Morisaki, H., and Itoh, N., 2001. “Correlation between the dielectric constant and porosity of nanoporous silica thin films deposited by the gas evaporation technique”. Applied Physics Letters, **79** (19) , pp. 3140–3142.

[30] Pap, A., Kordás, K., Vähäkangas, J., Uusimäki, A., Leppävuori, S., Pilon, L., and Szatmári, S., 2005. Optical properties of porous silicon. Part III: Comparison of experimental and theoretical results. submitted to Optical Materials.

[31] Ferrand, P., and Romestain, R., 2000. “Optical losses in porous silicon waveguides in the near-infrared: Effects of scattering”. *Applied Physics Letters*, **77** , pp. 3535–3537.

[32] Lerondel, G., and Romestain, R., 1997. “Quantitative analysis of light scattering effects on porous silicon optical measurements”. *Thin Solid Films*, **297** , pp. 114–117.

[33] Braun, M., and Pilon, L., 2005. “Effective optical properties of non-absorbing nanoporous thin-films”. *Thin Solid Films (in review)* .

[34] Kittel, C., 1996. *Introduction to Solid State Physics*. John Whiley and Sons.

[35] Jellison, G., and Modine, F., 1994. “Optical functions of silicon at elevated temperatures”. Journal of Applied Physics, **76** (6) , pp. 3758–3761.

[36] Manifacier, J., Gasiot, J., and Fillard, J., 1976. “A simple method for the determination of the optical constants n, k and the thickness of a weakly absorbing thin film”. *Journal of Physics E: Scientific Instruments*, **9** , pp. 1002–1004.

Copyright © 2005 by ASME